The Journal of Chemical Physics

Multidimensional spectroscopy of magneto-excitons at high magnetic fields

Cite as: J. Chem. Phys. **155**, 204201 (2021); https://doi.org/10.1063/5.0070113
Submitted: 03 September 2021 • Accepted: 02 November 2021 • Accepted Manuscript Online: 02 November 2021 • Published Online: 22 November 2021

V. Mapara, C. E. Stevens, J. Paul, et al.

The Journal of Chemical Physics ARTICLE scitation.org/journal/jcp

Multidimensional spectroscopy of magneto-excitons at high magnetic fields

Cite as: J. Chem. Phys. 155, 204201 (2021); doi: 10.1063/5.0070113
Submitted: 3 September 2021 • Accepted: 2 November 2021 •
Published Online: 22 November 2021

V. Mapara,[1] C. E. Stevens,[1] J. Paul,[1] A. Barua,[1] J. L. Reno,[2] S. A. McGill,[3] D. J. Hilton,[4] and D. Karaiskaj[1,a)]

AFFILIATIONS

[1] Department of Physics, University of South Florida, 4202 East Fowler Ave., Tampa, Florida 33620, USA
[2] CINT, Sandia National Laboratories, Albuquerque, New Mexico 87185, USA
[3] National High Magnetic Field Laboratory, Florida State University, Tallahassee, Florida 30201, USA
[4] Department of Physics, University of Alabama at Birmingham, Birmingham, Alabama 35294, USA

Note: This paper is part of the JCP Special Topic on Time-Resolved Vibrational Spectroscopy.
[a)] **Author to whom correspondence should be addressed:** karaiskaj@usf.edu

ABSTRACT

We perform two-dimensional Fourier transform spectroscopy on magneto-excitons in GaAs at magnetic fields and observe Zeeman splitting of the excitons. The Zeeman components are clearly resolved as separate peaks due to the two-dimensional nature of the spectra, leading to a more accurate measurement of the Zeeman splitting and the Landé g factors. Quantum coherent coupling between Zeeman components is observed using polarization dependent one-quantum two-dimensional spectroscopy. We use two-quantum two-dimensional spectroscopy to investigate higher four-particle correlations at high magnetic fields and reveal the role of the Zeeman splitting on the two-quantum transitions. The experimental two-dimensional spectra are simulated using the optical Bloch equations, where many-body effects are included phenomenologically.

I. INTRODUCTION

Optical excitations in semiconductors lead to excitons, the Coulomb bound electron–hole pairs. Excitons in GaAs are well explained by the Wannier theory.[1] An externally applied magnetic field will quantize the energies and angular momenta of the charged particles and thus change the electronic state of an exciton. The energy of each exciton state varies with the magnetic field depending on the basic exciton parameters. Therefore, magnetic fields provide a valuable tool to characterize various exciton properties, such as the effective mass, binding energy, Bohr radius, and Landé g-factor. The strength of the magnetic field compared to the exciton binding energy determines the energy shift of the exciton. Therefore, at relatively low magnetic fields where the effect of the Coulomb interaction is larger than that of the magnetic fields, one observes a quadratic shift of the exciton energy. Alternatively, in the high magnetic field limit where the effect of the external field dominates, the exciton states show a linear energy shift with magnetic fields, similar to free electron–hole pairs.[2,3]

In addition to the diamagnetic energy shift, the external magnetic fields lead to the Zeeman splitting of the excitons according to the electron spin and hole angular momenta. The energy shift of the electron and holes in a magnetic field is determined by its effective g factor. The free-electron spin splitting factor, of value $g = 2.0023$, defines the influence of the external magnetic field on the doublet of otherwise degenerate electron states with spin $s \pm 1/2$. However, the interaction of electron states with the lattice potential in crystals leads to a renormalization of the g factor value.[4,5] The correct determination of this splitting and its dependence on physical parameters is essential for a proper interpretation of optical experiments in magnetic fields. Furthermore, it could serve as an important tool in constructing theoretical models for the band structure and exciton mixing in bulk and two-dimensional materials. The difficulty in the optical determination of the exciton Zeeman splitting is that at small and moderate fields below 10 T, this splitting is smaller than the exciton linewidth. Therefore, it cannot be easily resolved using linear spectroscopy techniques.

The exchange interaction and Zeeman splitting of excitons in bulk GaAs and quantum wells have been studied both experimentally and theoretically.[6–10] The experimental studies include photoluminescence spectroscopy using circularly polarized light,[11] four-wave mixing (FWM) quantum beat spectroscopy[12] spin quantum

beats, measuring the transverse and longitudinal g factor in quantum wells, as well as overall dependence on the quantum well layer width and more details of the g factor anisotropy.[13–15] These studies showed that in GaAs quantum wells, the Landé g factor has a strong dependence on the quantum well width.

More recently, excitons in quantum dots[16] and monolayer transition metal dichalcogenides (TMDs)[17] have been the subject of study in high magnetic fields. Experimental studies of the magnetic field dependence of excitons in $MoSe_2$, WSe_2, WS_2[18–23] have been compared with theoretical $\mathbf{k} \cdot \mathbf{p}$[24] and first-principles calculations[25] of the Zeeman splitting in monolayer TMDs. The picture became more interesting when g factors of ~9.5 were experimentally observed for dark exciton states in bilayer WSe_2[26] and when interlayer excitons in heterobilayers of TMD where demonstrated to have g factors of ~6.7 and ~16,[27] which deviate even more from the value expected for ground state excitons in TMDs. Recent first-principle calculations conclude that due to specific optical selection rules, g factors in TMD heterostructures are strongly spin- and stacking dependent.[25]

Furthermore, external magnetic fields can distort the exciton and enhance higher order four-particle correlations.[28] The quantum coherence and correlations between excitons in undoped semiconductor quantum wells have been studied extensively using time-integrated, time-resolved, and spectrally resolved four-wave mixing (FWM) spectroscopy and have provided important insights into the many-body interactions taking place.[29–31] The time-resolved coherent spectroscopy provides unique tools to study the dynamics of strongly correlated systems, since it can probe direct contributions that occur as a result of four-particle and higher terms in perturbation theory. One excellent example of the role of many-body interactions is the appearance of a signal for "negative delay" in FWM experiments.[28,32–44] The occurrence of the FWM signal at negative delays is the result of four-particle correlations effects. The appearance of the four-particle induced negative delay signal becomes much more pronounced in bulk GaAs under magnetic fields, becoming equal to the "positive delay" signal at 10 T and showing a non-exponential rise. This surprising effect was attributed to non-Markovian memory effects.[32,34,35]

Recently, two-dimensional Fourier transform (2DFT) spectroscopy was developed and has provided new insights in the many-body physics of excitons in semiconductors.[44–53] The correlated nature of the frequency axes can reveal underlying physics in the form of two-dimensional line shapes and additional peaks in the 2DFT frequency spectra.[54] In this article, we perform 2DFT spectroscopy on the high quality bulk GaAs crystal at magnetic fields up to 10 T and perform theoretical simulations based on the optical Bloch equations in order to reproduce the experimental data. The S_1 2DFT spectra provide insight into the homogeneous linewidth of excitonic transitions at high magnetic fields, as well as the Zeeman splitting and the exciton g-factor. The two-dimensional nature of the spectra provides a much more convenient and clear method of measuring the Zeeman splitting and determining the g-factors. In order to further investigate the previously observed non-Markovian dynamics in the negative delay signal, we acquire S_3 2DFT spectra at different magnetic fields up to 10 T. We observe changes in the cross-peak intensities with increasing magnetic fields and attribute it to the Zeeman splitting of the excitons. These changes are well reproduced using the optical Bloch equations.

II. EXPERIMENT AND SAMPLES

The experimental setup used in the present study is shown in Fig. 1(a). Three laser pulses are incident on the sample in directions $\vec{k}_a$, $\vec{k}_b$, and $\vec{k}_c$ separated by the time delays τ and T, and the FWM signal evolves during the time t [Figs. 1(b) and 1(c)]. The third-order nonlinear interaction gives rise to a signal in the direction $-\vec{k}_a + \vec{k}_b + \vec{k}_c$. By varying the time delay τ and monitoring the FWM intensity, referred to as time integrated FWM, the dephasing time of excitons can be measured. In 2DFT spectroscopy, the time delays τ or T and t are monitored simultaneously while scanning with interferometric precision and accurately preserving the phase. The Fourier transform to the frequency domain with respect to the two time delays τ and t leads to correlated two-dimensional frequency spectra dependent on ω_τ and ω_t.[57,58] When the spectra are plotted with respect to $-\omega_\tau$ and ω_t, the resonances probed appear along the diagonal, whereas signatures of quantum coherent coupling can be manifested as cross-diagonal peaks.[59] Furthermore, the two-dimensional line shapes are highly sensitive to the many-body interactions in the sample, making this technique very suited to study many-body effects.

By varying the "positive" time delay τ in Fig. 1(b) and monitoring the FWM intensity, referred to as time integrated FWM, the dephasing time of excitons can be measured. When the phase conjugate pulse A^* arrives at the sample last, the "negative" time delay leads to two-quantum coherences [Fig. 1(c)]. In order to generate the 2DFT spectra, a Fourier transform is performed with respect to two of the time variables, while the third is held constant. For the "positive" delay signal, the Fourier transform leads to 2DFT spectra in the frequency domain described by $S_1(\omega_\tau, T, \omega_t)$, whereas for the "negative" delay signal, two-quantum coherences appear in the $S_3(\tau, \omega_T, \omega_t)$ spectra. The advantages of multidimensional spectroscopy are well documented in the literature,[57,60–65] where in semiconductor nanomaterials, 2DFT spectroscopy has provided insights into the microscopic details of the many-body interactions.[46,48,53]

The laser pulses with a duration ~130 fs were generated by a standard tunable Ti:sapphire oscillator. The sample was held at 1.6 K inside the Oxford Spectromag magneto-optical cryostat. The magnetic field was applied in the Faraday geometry perpendicular to the sample surface and could be varied from zero up to 10 T. The sample consists of an ultra pure 200 nm thick GaAs layer grown by molecular beam epitaxy (VB0915).

III. RESULTS AND DISCUSSION

In bulk GaAs, the $J_h = 1/2$ and $J_h = 3/2$ valence band states are split by the spin–orbit interactions. The $J_h = 3/2$ top valence band states are fourfold degenerate and belong to the Γ_8 symmetry group, whereas the electron states at the conduction band minimum are twofold spin degenerate and belong to Γ_6 group. The symmetry of the lowest 1*s* exciton in bulk GaAs at the Γ point is determined by the direct product of the Γ_6 ($S = 1/2$) conduction electron and the Γ_8 ($J_h = 3/2$) valence hole, leading to the following irreducible representations $\Gamma_6 \otimes \Gamma_8 = \Gamma_5 \oplus \Gamma_4 \oplus \Gamma_3$. In the *J*–*J* coupling scheme for excitonic states, the first term corresponds to states with total angular momentum $J = 1$ and the latter two correspond to states with $J = 2$. The electron–hole exchange interaction lift the degeneracy between the Γ_5 and the Γ_4, Γ_3 states, or the $J = 1$ and $J = 2$ excitonic

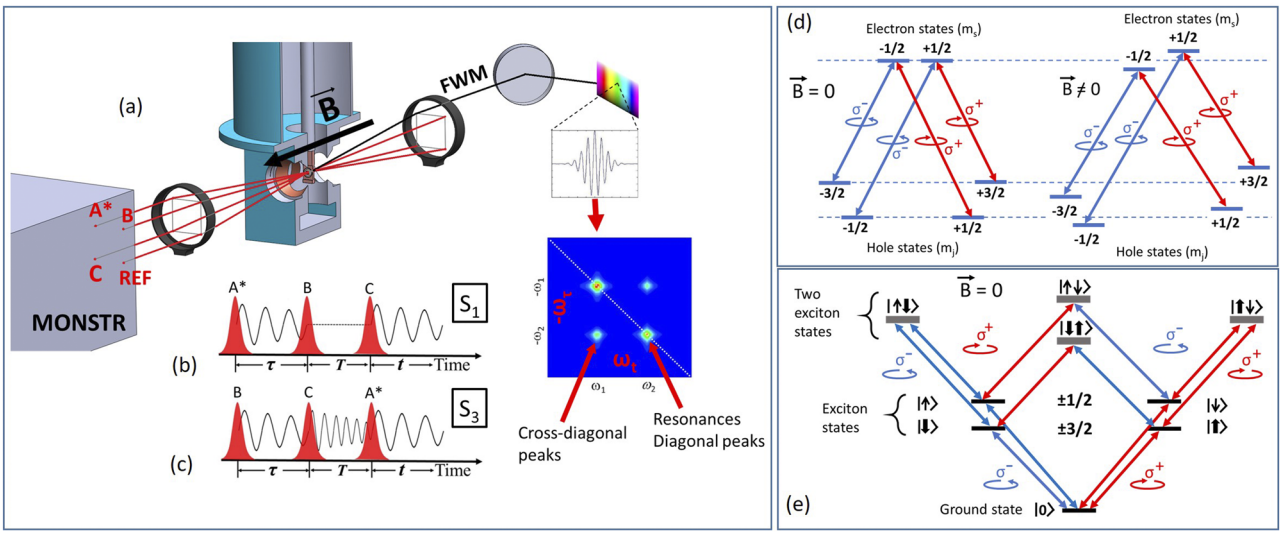

FIG. 1. (a) Schematic of the experimental setup: The four phase-stabilized laser beams are provided by the MONSTR instrument.[55,56] Three beams labeled as A*, B, and C are used to generate the FWM signal, where A* corresponds to the phase conjugate beam. The beams are aligned in the three corners of a square. The FWM signal generated at the sample propagates along the missing corner (direction $-\vec{k}_a + \vec{k}_b + \vec{k}_c$). A fourth beam labeled as Ref. is used to trace the FWM and as the local oscillator for heterodyne detection. The samples are kept at 1.6 K inside the magneto-optical cryostat (VB0915). Magnetic fields up to 10 T are applied perpendicular to the sample surface in Faraday geometry. The FWM signal is heterodyne detected and dispersed into a spectrometer. The Fourier transformed spectral interferograms lead to the 2DFT spectra. (b) Pulse sequence leading to the S_1 2DFT signal ($-\vec{k}_a + \vec{k}_b + \vec{k}_c$). (c) When the phase conjugate pulse A* arrives last, the S_3 2DFT signal is obtained, corresponding to the direction $\vec{k}_a + \vec{k}_b - \vec{k}_c$. (d) The level scheme for the $m_h = \pm 3/2$ and $m_h = \pm 1/2$ excitons in bulk GaAs. In the absence of magnetic fields, the degeneracy between the $m_h = \pm 3/2$ and $m_h = \pm 1/2$ excitons is lifted by the external strain. Magnetic fields further lift the degeneracy between the $m_h = +3/2$ and $m_h = -3/2$ ($m_h = +1/2$ and $m_h = -1/2$) excitons. The blue and red arrows represent excitations with σ^- and σ^+ circularly polarized light. (e) The "W-diagram" includes exciton and two-exciton (four-particle) states in the absence of magnetic fields showing the different pathways that excitons and two-exciton states can be formed using σ^- and σ^+ circularly polarized light. It can lead to two $m_h = \pm 3/2$ or $m_h = \pm 1/2$ exciton states or mixed two-exciton states.

states, where in the absence of external perturbations, the $J = 1$ is optically allowed and the $J = 2$ is forbidden.[66,67]

The electron–hole exchange interaction splitting between the $J = 1$ and $J = 2$ has been measured experimentally and calculated theoretically. The measured values of the exchange interaction splitting vary between 20 and 370 μeV.[68–70] External perturbations such as magnetic fields can mix the states and $J = 2$ states can become allowed. The magnetic fields also lead to the Zeeman splitting of the excitonic m_J components, which are polarization dependent and can be selectively excited. In the Faraday configuration, two transitions belonging to the $J = 1$ exciton and two transitions belonging to the $J = 2$ each with $m_J = \pm 1$ can be selectively excited with $\sigma^{\pm}$ circularly polarized light.[71–77]

External strain shifts the electronic bands, lowers the crystal symmetry, and splits the valence $J_h = 3/2$ band at the $\Gamma-$ point into $|J_h = 3/2, m_h = \pm 3/2\rangle$ and $|J_h = 3/2, m_h = \pm 1/2\rangle$ states.[78–80] Holes from these bands now can form excitons with conduction band electrons, where each exciton is composed of a $m_h = \pm 3/2$ or $m_h = \pm 1/2$ hole and one $m_S = \pm 1/2$ electron. At zero magnetic fields, the $|J_h = 3/2, m_h = \pm 3/2\rangle$ and the $|J_h = 3/2, m_h = \pm 1/2\rangle$ excitonic states are degenerate. At finite magnetic fields, in addition to the diamagnetic energy shift, the degeneracy of the m_h excitonic states is lifted. In the Faraday configuration, four allowed transitions, two with $m_J = +1$ and two with $m_J = -1$, can be selectively excited using circular polarizations, where m_J here refers to the exciton total angular momentum projections. These four excitonic transitions are schematically shown in Fig. 1(d) at zero and finite magnetic fields. Furthermore, exciton and two-exciton transitions are shown in Fig. 1(e) in the absence of external magnetic fields.

In our sample, we would expect one strong transition belonging to the free exciton, but in the S_1 2DFT spectra at (H, H, H, H) polarizations, we observe two peaks with a ~2.5 meV splitting between a stronger peak, labeled as A, and a weaker peak B. These peaks fall along the diagonal of the 2DFT spectra in Fig. 2(a). A strong and a weak feature can be observed in the absorption and FWM spectra plotted above. The expected fine structure splitting between the $J = 1$ and $J = 2$ excitons due to the electron–hole exchange interactions is in the sub meV range.[68–70] The energy position of the 1*s* state of the free exciton was accurately measured and reported at ~1.5153 eV and that of the 2*s* excited state ~3.2 meV higher at ~1.5185 meV, leading an exciton binding energy of ~4.2 meV and a lowest direct bandgap energy of ~1.5195 meV.[71,74,81] The observation of the lowest excitonic state peak A at somewhat higher energy (~1.5175 eV), and the somewhat arbitrary splitting of peaks A and B indicates the presence of external strain in our sample, likely originating from the substrate removal and mounting on the quartz substrate.[82,83]

A. Theoretical simulations

The FWM signal is a result of the third order nonlinear polarization of the material $P^{(3)} = \chi^{(3)}E^3$ (omitting the vector and tensor notation), where $\chi^{(3)}$ is the third order non-linear susceptibility and

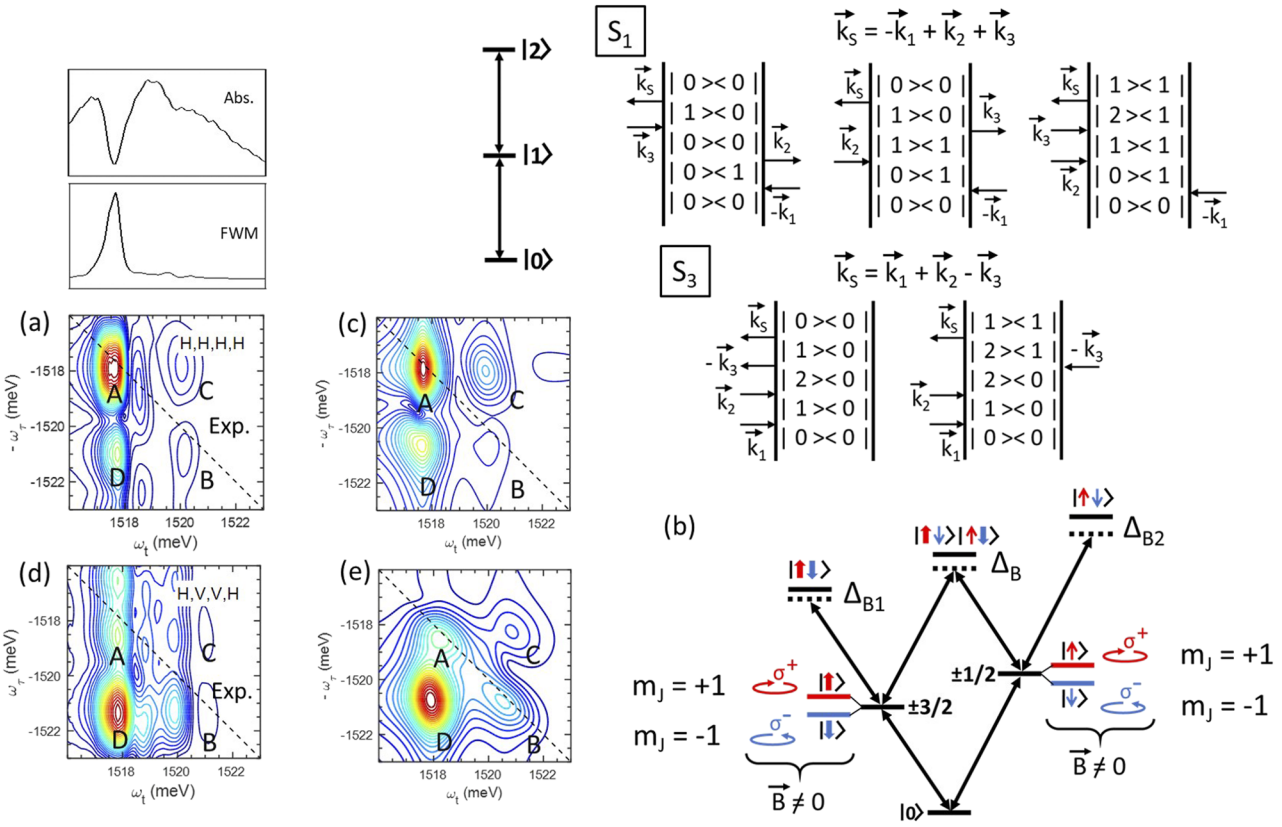

FIG. 2. Experimental S_1 2DFT spectra at different polarizations (a) (HHHH) and (d) (HVVH), where the polarizations correspond to A*, B, C, and detection, respectively. The spectrally resolved FWM and the absorption (Abs.) are shown above the experimental 2DFT spectra. (b) Double-sided Feynman diagrams contributing to the S_1 and S_3 signals. The state $|0\rangle$ corresponds to the semiconductor ground state, the state $|1\rangle$ corresponds to exciton state, and the state $|2\rangle$ corresponds to the two-exciton four-particle state. The "W-diagram" used in the simulations takes into account the two types of excitons with $m_h = \pm 3/2$ and $m_h = \pm 1/2$ with different energies and their spins. The m_h degeneracy is lifted at finite magnetic fields and circular polarizations can be used to access the individual spin states. The diagram includes two branches for the $m_h = \pm 3/2$ and $m_h = \pm 1/2$ excitons and mixed exciton states. Many-body interactions are included phenomenologically by introducing an energy shift of the two-exciton states, labeled in the diagram as Δ_{B1}, Δ_{B2}, and Δ_B, for the two $m_h = \pm 3/2$ exciton, the two $m_h = \pm 1/2$ exciton, and mixed two-exciton states, respectively. (c) and (e) Theoretical spectra calculated using the optical Bloch equations where many-body effects such as EID and EIS are included phenomenologically for the (HHHH) and (HVVH) polarizations, respectively.

E^3 are three incident electrical fields. In our experiment, the electric fields E are provided by three incident laser pulses. The field of each laser pulse can be expressed as $E_i(\mathbf{r},t) = \hat{E}_i e^{i(\mathbf{k}_i\mathbf{r}-\omega_i t)} + c.c.$, where $\hat{E}_i$, $\mathbf{k}_i$, and ω_i are the field envelope, wavevector, and angular frequency of the ith pulse. The total field generating the third order polarization $P^{(3)}$ is the sum of the three incident pulses: $E(\mathbf{r},t) = \sum_i E_i(\mathbf{r},\omega_i, t - t_i)$, where the ith laser pulse arrives at time t_i. The material's response is essential in generating the third order polarization and is contained in the third order susceptibility $\chi^{(3)}$.

An equivalent form of writing the third order polarization $P^{(3)}$ that explicitly contains the time ordering of the laser pulses is given in the time domain by

$$P^{(3)}(\mathbf{r},t) = \int_0^\infty dt_3 \int_0^\infty dt_2 \int_0^\infty dt_1 R^{(3)}(t_3,t_2,t_1) E(\mathbf{r},t-t_3) \times E(\mathbf{r},t-t_3-t_2) E(\mathbf{r},t_3-t_2-t_1), \quad (1)$$

where $R^{(3)}$ is the third order response function that contains the interactions of the light fields with the material system, including the material's optical dipole moments μ, transitions frequencies, and excited state dynamics. The description via the response function provides a convenient way to describe the light–mater interactions in terms of Liouville space double-sided Feynman diagrams. In the limit of impulsive excitation, where the pulse duration is short compared to the system dynamics and the pulse delays, each pulse can be approximated by a delta function. This approximation together with choosing a certain phase matching condition (S_1) $-\vec{k}_a + \vec{k}_b + \vec{k}_c$ and (S_3) $\vec{k}_a + \vec{k}_b - \vec{k}_c$, which can be achieved by simply changing the laser pulse ordering, further simplifying the calculation of $P^{(3)}$ in Eq. (1), by reducing the number of Feynman diagrams that contribute to each technique.

Density matrix theory is the method of choice in treating experiments using ultrashort laser pulses because it provides dynamic

variables that are directly related to observables. The density matrix formulation can be used to simulate the third order response of the system and to generate sum-over-states expressions for the response function $R^{(3)}$. In the dipole approximation, the equations of motion for the density matrix ρ are the optical Bloch equations, which can be derived from the Liouville equation,

$$i\hbar\frac{d\rho}{dt} = [\hat{H}, \rho], \tag{2}$$

where H is the total Hamiltonian including the light–matter interaction given by $-\mu E(\mathbf{r}, t)$. The inclusion of the Coulomb interactions and the resulting semiconductor Bloch equations are crucial in describing the nonlinear optical response of semiconductors, leading to excitation induced shift (EIS) and excitation induced dephasing (EID). In the present work, we solve the optical Bloch equations and include EIS and EID phenomenologically due to the complexity of solving the semiconductor Bloch equations. Each quantum pathway of the optical Bloch equations can be conveniently described by a double-sided Feynman diagram, describing the time evolution of the density matrix. The Feynman diagrams for a ladder diagram that includes one and two excitons states are shown in Fig. 2(b) for the S_1 and S_3 technique. For the S_1 technique, where the phase conjugate pulse A^* $(-\vec{k}_1)$ arrives at the samples first, the evaluation of the optical Bloch equations leads the three double-sided Feynman diagrams, known as ground-state bleaching, excited-state emission, and excited state absorption, from left to right, respectively.

These diagrams are applied to the W-diagram shown in the same Fig. 2(b), which includes two branches for the $m_h = \pm 3/2$ and $m_h = \pm 1/2$ excitons and mixed exciton states. Many-body interactions are included phenomenologically by introducing an energy shift of the two-exciton states, labeled in the diagram as Δ_{B1}, Δ_{B2}, and Δ_B, for the two $m_h = \pm 3/2$ exciton, the two $m_h = \pm 1/2$ exciton, and mixed two exciton states, respectively. This scheme has been used in the past to simulate the 2DFT spectra of excitons in bulk GaAs and quantum wells.[46,84–87] Furthermore, we include the effects of magnetic fields, which lift the degeneracy between the $m_J = +1$ and $m_J = -1$ excitons. The Zeeman splitting of the $m_h = \pm 3/2$ and $m_h = \pm 1/2$ excitons in magnetic fields into $m_J = +1$ and $m_J = -1$ excitons and their coupling are included in the simulation.

The S_3 technique, where the phase conjugate pulse A^* $(-\vec{k}_3)$ arrives at the sample last, leads to two-quantum transitions described by the two Feynman diagrams shown in Fig. 2(b). These are applied to the W-diagram by taking into account all different pathways, two-quantum $m_h = \pm 3/2$, two-quantum $m_h = \pm 1/2$, and mixed excitons in order to simulate the two-quantum 2DFT spectra in Fig. 6. The equal splitting of the $m_J = +1$ and $m_J = -1$ excitons in magnetic fields is assumed to mutually cancel out at the two-exciton level.

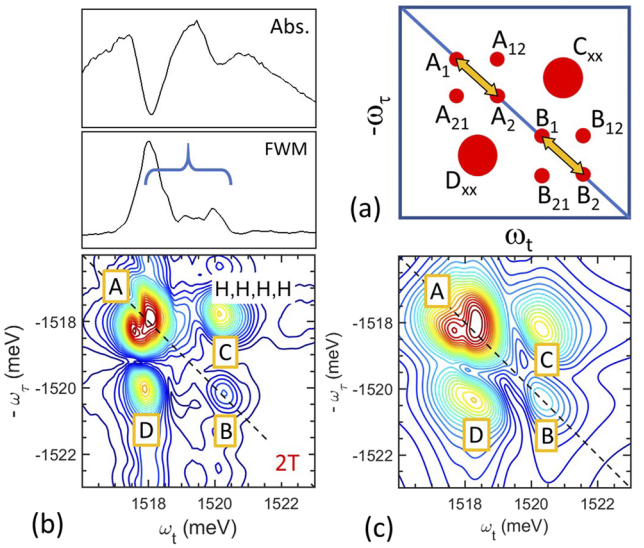

FIG. 3. (a) Schematic of the peak structure of the 2DFT spectra. The A and B labeled peaks represent the heavy and light hole excitonic resonances, respectively. The C and D labeled peaks correspond to the anticipated cross peaks. (b) S_1 2DFT spectra at magnetic fields of 2 T and polarizations (HHHH), where the polarizations correspond to A*, B, C, and detection, respectively. The spectrally resolved FWM and the absorption (Abs.) are shown above the experimental 2DFT spectra. (c) Theoretical spectra calculated using the optical Bloch equations where many-body effects such as EID and EIS are included phenomenologically.

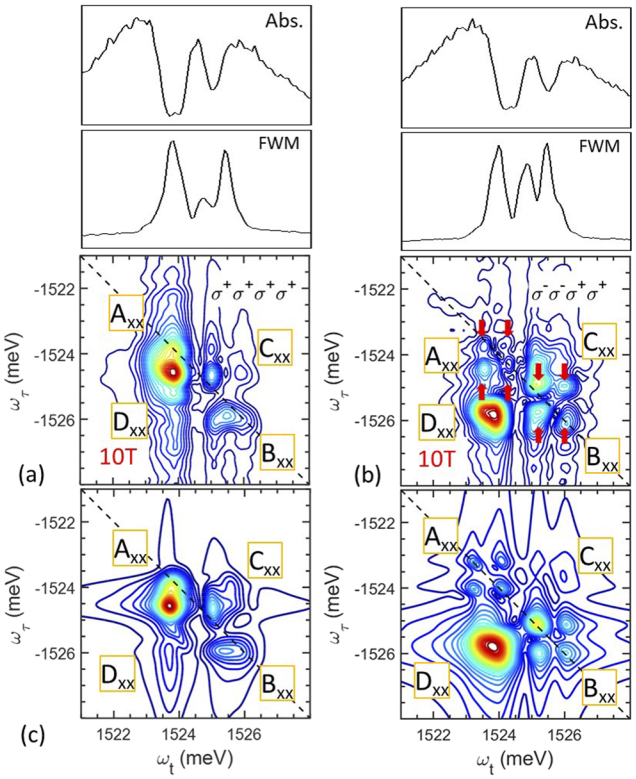

FIG. 4. (a) and (b) Experimental S_1 2DFT spectra at 10 T and with $(\sigma^+\sigma^+\sigma^+\sigma^+)$ and $(\sigma^-\sigma^-\sigma^+\sigma^+)$ polarizations, where the polarizations correspond to A*, B, C, and detection, respectively. The spectrally resolved FWM and the absorption (Abs.) are shown above the experimental 2DFT spectra. (c) and (d) Calculated S_1 2DFT spectra at 10 T and with $(\sigma^+\sigma^+\sigma^+\sigma^+)$ and $(\sigma^-\sigma^-\sigma^+\sigma^+)$ polarizations using the optical Bloch equations, where many-body effects such as EID and EIS are included phenomenologically.

B. One-quantum 2DFT spectra

Excitons in bulk GaAs under magnetic fields are expected to experience diamagnetic energy shift and Zeeman splitting of the total angular momentum projections. The diamagnetic shift leads to an energy shift of excitons for both orbital angular momentum projections $m_j = \pm 1$.[88] Electrons and holes have spin and orbital angular momentum, and therefore, excitons will experience a finite magnetic dipole moment in external magnetic fields, proportional to the projection of the angular momentum m_J. This leads to the Zeeman splitting of the energy levels, with an energy shift proportional to $g\mu_B \mathbf{B} m_J$, where g is the Landé factor, μ_B is the Bohr magneton, and $\mathbf{B}$ is the magnetic field. Considering the total angular momentum of the $m_h = \pm 3/2$ and $m_h = \pm 1/2$ excitons, the optically allowed excited states require the total angular momentum projections to be $m_J = \pm 1$. Therefore, at high fields, the $m_h = \pm 3/2$ and $m_h = \pm 1/2$ excitons should experience similar Zeeman splitting, differing by the Landé factors g, which are renormalized for electrons and holes in solids.

We continue our discussion with the S_1 2DFT spectra at zero magnetic fields shown in Fig. 2. The size of the splitting between the $m_h = \pm 3/2$ excitons labeled as peak A and $m_h = \pm 1/2$ excitons labeled as peak B depends on the strength and nature of the strain and thus will not be discussed.[78,79,82,89–91] The 2DFT data are collected for two different polarizations (H, H, H, H) and (H, V, V, H), where each polarization corresponds to A*, B, C, and detection, respectively. The 2DFT spectra is consistent with what has been observed in bulk GaAs without magnetic fields, and the polarization (H, V, V, H), referred to here as cross-linear, enhances the cross peaks labeled in Fig. 2 as C and D.[82] The experimental data have been simulated for both polarizations using the optical Bloch equations, where many-body effects such as EIS and EID have been included phenomenologically.

At 2 T, the measured S_1 2DFT spectra at (H, H, H, H) polarizations are shown in Fig. 3(b). The horizontal polarizations do not favor any particular transition in the W-diagram in Fig. 1(e). We observe a narrowing of the diagonal and cross-diagonal peaks in the 2DFT spectra, and a splitting of the $m_h = \pm 3/2$ exciton peak A starts to appear. Two cross-diagonal peaks labeled as C and D indicate quantum coherent coupling between $m_h = \pm 3/2$ and $m_h = \pm 1/2$ excitons in the 2DFT spectra. The absorption spectra shown in the same figure show only two peaks, whereas the FWM reveals more structure in the area marked by the blue bracket. A schematic of the expected peak structure due to the Zeeman splitting is shown in Fig. 3(a). The ability to resolve the subcomponents depends on the size of the Zeeman splitting and width of the transitions. However, the ability of the 2DFT technique to spread the resonance and coupling peaks in the two-dimensional Fourier plane provides clear advantages in identifying the underlying Zeeman components. The Zeeman splitting depends on exciton angular momentum projection m_J and magnetic field $\mathbf{B}$. In Fig. 3, the 2DFT peaks have been labeled as A_{xx}, B_{xx}, C_{xx}, and D_{xx}, where the subscript corresponds to the Zeeman subcomponents.

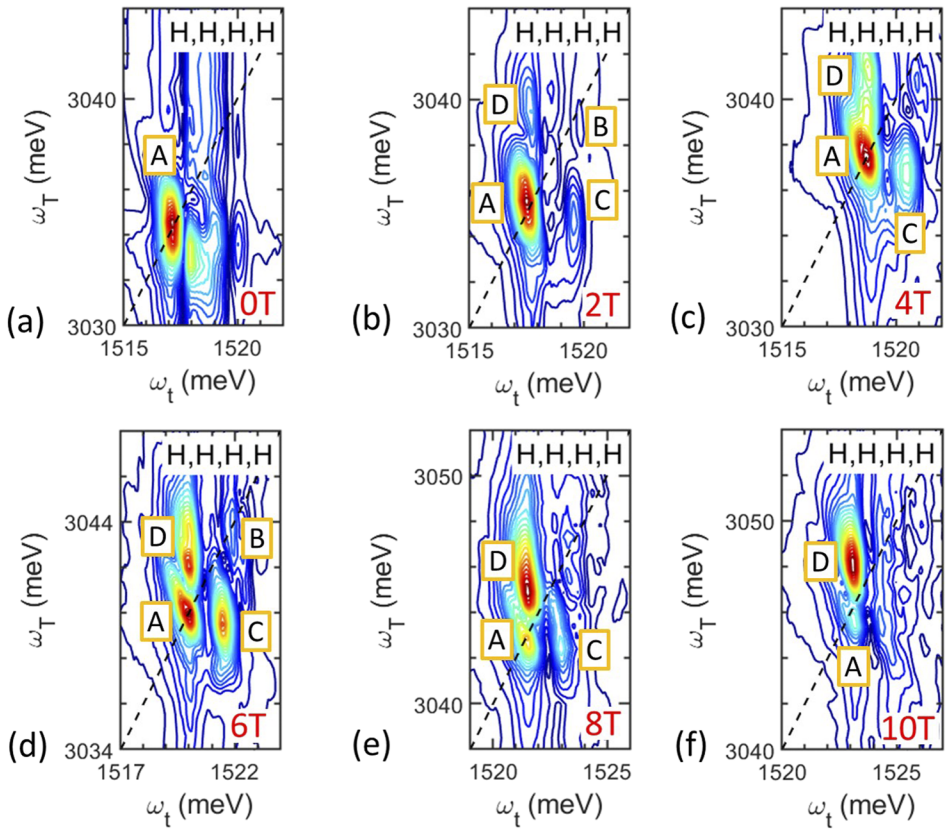

FIG. 5. (a)–(e) Experimental S_3 2DFT spectra at (HHHH) polarizations as a function of magnetic fields, at 0, 2, 4, 6, 8, and 10 T, respectively. The ω_T axis is twice the ω_t axis, reflecting two-quantum transitions.

Spectrally resolved and time-integrated FWM can provide only limited insights into the underlying Zeeman splitting. In the absorption, only the two main $\pm 3/2$ and $m_h = \pm 1/2$ exciton peaks can be observed. The spectrally resolved FWM does provide some indication to the Zeeman splitting, with additional peaks appearing marked by the bracket, but the peak structure is very difficult to disentangle. Exciting an excitonic system subjected to a magnetic field, with a linearly polarized pulse that has larger spectral width than the Zeeman splitting, creates a superposition of the two excitonic states. In a FWM experiment, this gives rise to deep temporal oscillations in the emitted signal, reflecting quantum beats between the two states. Quantum coherence between excitons in GaAs was first observed as quantum beating in the FWM decay. However, one-dimensional FWM spectroscopy could not unambiguously distinguish between quantum and polarization beating. It is the advent 2DFT spectroscopy that could differentiate between the two processes.[59] In the present study, 2DFT spectroscopy reveals the full picture, including the strong quantum coherent coupling between the Zeeman components and all the couplings and relaxation pathways between transitions. The experimental 2DFT data have been simulated by introducing additional resonances in the original theoretical model according to Fig. 2(b) in order to account for the Zeeman splitting. The simulated 2DFT spectra are shown in Fig. 3(c), and the relative peak intensities and the two-dimensional line shapes are well reproduced by the simulated 2DFT spectra.

Increasing the magnetic field leads to larger Zeeman splitting and narrower lines. At 10 T, the structure of the Zeeman components becomes apparent. The co-circular ($\sigma^+\sigma^+\sigma^+\sigma^+$) polarization sequence is shown in Fig. 4(a). The co-circular polarizations suppress the cross-diagonal peaks and enhance the diagonal peaks. The simulated 2DFT spectra are shown in Fig. 4(c). The overlap between the peaks can shift their center position and complicate their assignment. The overlap between close lying peaks can alter the relative intensity of the peaks. It is the cross-circular ($\sigma^-\sigma^-\sigma^+\sigma^+$) polarization sequence in (Fig. 4) (b) that suppresses the diagonal peaks, thus enhancing the cross peaks that reveals the underlying Zeeman splitting and the quantum coherent coupling between the Zeeman components. The four peaks for the heavy and light holes are labeled as A_{xx} and B_{xx} and are marked by red arrows. The two peaks along the diagonal, which were labeled as A_1 and A_2 or B_1 and B_2 in Fig. 3(a), correspond to the Zeeman components, whereas the cross-diagonal peaks labeled as A_{12} and A_{21} or B_{12} and B_{21} in the same picture indicate quantum coherent coupling between the two Zeeman components.[57] The combination of the multidimensional nature of

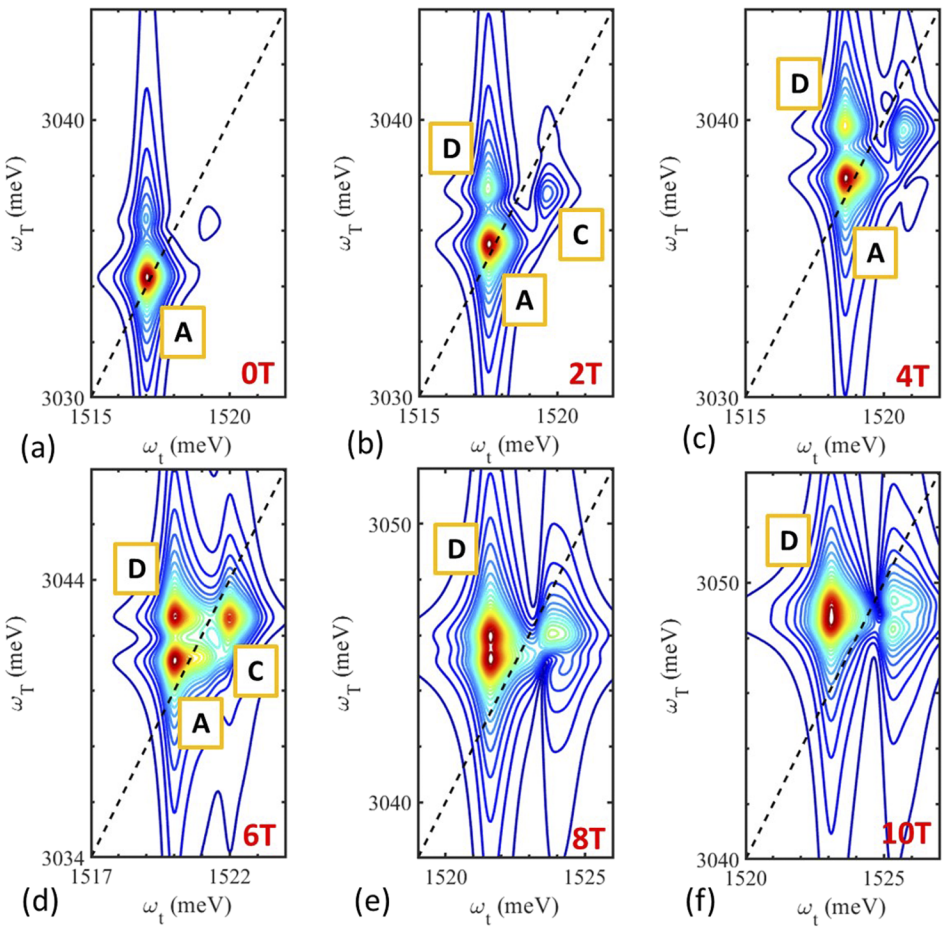

FIG. 6. (a)–(e) Simulated S_3 2DFT spectra at (HHHH) polarizations as a function of magnetic fields, at 0, 2, 4, 6, 8, and 10 T, respectively. The ω_T axis is twice the ω_t axis, reflecting two-quantum transitions.

2DFT spectroscopy with polarization selection can reveal the full underlying peak structure, which is not obtainable in the spectrally resolved FWM and absorption spectra shown in Fig. 4 above the 2DFT spectra.

The measured Zeeman splitting for the $m_h = \pm 3/2$ exciton is ~0.7 meV and the $m_h = \pm 1/2$ exciton is ~0.8 meV. These values lead to g factors of ~1.2 and ~1.4, respectively. In the S_1 2DFT spectra, the profile of the resonance along diagonal line, marked by the dashed black line in Fig. 4, provides the inhomogeneous linewidth of the excitonic transition. The inhomogeneous excitonic linewidth is what is usually obtained in absorption, photoluminescence, or spectrally resolved FWM. It is dominated by the Gaussian distribution of frequencies due to the imperfections of the GaAs crystal. We measure an inhomogeneous linewidth of ~0.6 meV, which emphasizes the high quality of the GaAs crystal. The cross-diagonal profile of the resonance provides the homogeneous linewidth of the exciton transitions.[92] We obtain homogeneous linewidths of ~0.5 and ~0.6 meV for the $m_h = \pm 3/2$ and $m_h = \pm 1/2$ excitons at zero and low magnetic fields, respectively. The homogeneous linewidth is reduced to ~0.3 and ~0.4 meV at 10 T for the $m_h = \pm 3/2$ and $m_h = \pm 1/2$ excitons, respectively.

C. Two-quantum 2DFT spectra

In order to further explore the non-Markovian dynamics observed previously on the negative delay FWM signal,[33,34] we proceed by discussing the S_3 two-quantum 2DFT spectra. The increase in the negative delay FWM signal accompanied by the non-exponential rise was attributed to enhanced exciton–exciton correlations due to the external magnetic field. The S_3 two-dimensional line shape does provide insights into the degree of four-particle correlation in the system.[93] The S_3 2DFT spectra for the (H, H, H, H) polarization sequence is shown in Fig. 5 for several magnetic fields. The S_3 signal is due to four-particle correlations and requires two magneto-excitons to generate a two-quantum transition. However, the negative delay signal can originate from unbound exciton–exciton correlations or from bound biexcitons.[28,46,85–87] The exciton binding energy in bulk GaAs is ~4.2 meV, which would lead to a small biexciton binding energy. The biexciton peak would appear shifted off the diagonal from peak A in Figs. 5(a)–5(f). Instead, peak A appears as a single peak at all magnetic fields, indicating that it originates from exciton–exciton correlations.

Peak A, which originates from two $m_h = \pm 3/2$ excitons, dominates the spectra at zero and low fields. Peak B originating from the $m_h = \pm 1/2$ excitons is much weaker due to the center frequency of the exciting laser and its lower oscillator strength. With increasing magnetic fields, cross peaks C and D become stronger, and at the highest field of 10 T, cross peak D dominates the 2DFT spectra. The line shapes of the S_3 2DFT peaks indicate a large degree of correlation.[93] We model the effect of the external magnetic fields on the two-exciton transitions by incorporating the Zeeman splitting of the individual $m_h = \pm 3/2$ and $m_h = \pm 1/2$ excitons. We simulate the effect of the magnetic fields by energetically shifting states of opposite spins in opposite directions. The Zeeman effect on the two-exciton states leads to a progressive strengthening of cross peak D in the S_3 2DFT spectra with increasing magnetic fields. The simulated 2DFT spectra at the different magnetic fields are shown in Fig. 6 up to 10 T.

IV. CONCLUSIONS

We perform one-quantum S_1 and two-quantum S_3 2DFT spectroscopy on magneto-excitons at magnetic fields up to 10 T and at 1.6 K. The polarization dependent S_1 2DFT spectra reveal a Zeeman splitting of the $m_h = \pm 3/2$ and $m_h = \pm 1/2$ excitons. The one-dimensional spectroscopies such as absorption and spectrally resolved FWM obscure the Zeeman components. It is the two-dimensional nature of the 2DFT that facilitates the accurate measurement of the Zeeman splitting, leading to Landé g-factors of ~1.2 and ~1.4 for the $m_h = \pm 3/2$ and $m_h = \pm 1/2$ excitons, respectively. Furthermore, quantum coherent coupling is observed between the Zeeman components, revealed by their cross diagonal peaks A_{12} and A_{21} for the $m_h = \pm 3/2$ exciton and B_{12} and B_{21} for the $m_h = \pm 1/2$ exciton. Furthermore, the two-quantum S_3 2DFT spectra reveal changes in the peak intensities with increasing magnetic fields. These changes were attributed to the effect of the Zeeman splitting on the two-exciton transitions and were modeled by energetically shifting states of opposite spins in opposite directions. The experimental 2DFT spectra are well reproduced by the simulated response using the optical Bloch equations, where many-body effects are included phenomenologically.

ACKNOWLEDGMENTS

The work at USF and UAB was, in part, supported by the National Science Foundation under Grant No. DMR-1409473. This work was, in part, supported by the U.S. Department of Energy, Office of Basic Energy Sciences, Division of Materials Sciences and Engineering (Award No. DE-SC0012635). This work was performed, in part, at the Center for Integrated Nanotechnologies, an Office of Science User Facility operated for the U.S. Department of Energy (DOE) Office of Science by Los Alamos National Laboratory (Contract No. 89233218CNA000001), and Sandia National Laboratories (Contract No. DE-NA-0003525). A portion of this work was performed at the National High Magnetic Field Laboratory, which was supported by National Science Foundation Cooperative Agreement No. DMR-1157490 and the State of Florida.

AUTHOR DECLARATIONS

Conflict of Interest

The authors have no conflicts to disclose.

DATA AVAILABILITY

The data that support the findings of this study are available from the corresponding author upon reasonable request.

REFERENCES

[1] G. H. Wannier, Phys. Rev. **52**, 191 (1937).
[2] R. J. Elliott and R. Loudon, J. Phys. Chem. Solids **15**, 196 (1960).
[3] G. J. Rees, J. Phys. C: Solid State Phys. **5**, 549 (1972).
[4] L. M. Roth, B. Lax, and S. Zwerdling, Phys. Rev. **114**, 90 (1959).
[5] L. M. Roth, Phys. Rev. **118**, 1534 (1960).
[6] G. E. W. Bauer and T. Ando, Phys. Rev. B **37**, 3130 (1988).
[7] P. Lefebvre, B. Gil, J. P. Lascaray, H. Mathieu, D. Bimberg, T. Fukunaga, and H. Nakashima, Phys. Rev. B **37**, 4171 (1988).
[8] M. J. Snelling, E. Blackwood, C. J. McDonagh, R. T. Harley, and C. T. B. Foxon, Phys. Rev. B **45**, 3922 (1992).

[9]T. Wimbauer, K. Oettinger, A. L. Efros, B. K. Meyer, and H. Brugger, Phys. Rev. B **50**, 8889 (1994).
[10]E. L. Ivchenko, A. Y. Kaminski, and U. Rössler, Phys. Rev. B **54**, 5852 (1996).
[11]E. Blackwood, M. J. Snelling, R. T. Harley, S. R. Andrews, and C. T. B. Foxon, Phys. Rev. B **50**, 14246 (1994).
[12]O. Carmel, H. Shtrikman, and I. Bar-Joseph, Phys. Rev. B **48**, 1955 (1993).
[13]X. Marie, T. Amand, P. Le Jeune, M. Paillard, P. Renucci, L. E. Golub, V. D. Dymnikov, and E. L. Ivchenko, Phys. Rev. B **60**, 5811 (1999).
[14]A. A. Kiselev, K. W. Kim, and E. Yablonovitch, Phys. Rev. B **64**, 125303 (2001).
[15]I. A. Yugova, A. Greilich, D. R. Yakovlev, A. A. Kiselev, M. Bayer, V. V. Petrov, Y. K. Dolgikh, D. Reuter, and A. D. Wieck, Phys. Rev. B **75**, 245302 (2007).
[16]J. van Bree, A. Y. Silov, P. M. Koenraad, M. E. Flatté, and C. E. Pryor, Phys. Rev. B **85**, 165323 (2012).
[17]G. Wang, L. Bouet, M. M. Glazov, T. Amand, E. L. Ivchenko, E. Palleau, X. Marie, and B. Urbaszek, 2D Mater. **2**, 034002 (2015).
[18]Y. Li, J. Ludwig, T. Low, A. Chernikov, X. Cui, G. Arefe, Y. D. Kim, A. M. van der Zande, A. Rigosi, H. M. Hill, S. H. Kim, J. Hone, Z. Li, D. Smirnov, and T. F. Heinz, Phys. Rev. Lett. **113**, 266804 (2014).
[19]D. MacNeill, C. Heikes, K. F. Mak, Z. Anderson, A. Kormányos, V. Zólyomi, J. Park, and D. C. Ralph, Phys. Rev. Lett. **114**, 037401 (2015).
[20]A. Srivastava, M. Sidler, A. V. Allain, D. S. Lembke, A. Kis, and A. Imamoğlu, Nat. Phys. **11**, 141 (2015).
[21]A. V. Stier, N. P. Wilson, K. A. Velizhanin, J. Kono, X. Xu, and S. A. Crooker, Phys. Rev. Lett. **120**, 057405 (2018).
[22]S.-Y. Chen, Z. Lu, T. Goldstein, J. Tong, A. Chaves, J. Kunstmann, L. S. R. Cavalcante, T. Woźniak, G. Seifert, D. R. Reichman, T. Taniguchi, K. Watanabe, D. Smirnov, and J. Yan, Nano Lett. **19**, 2464 (2019).
[23]J. Zipfel, J. Holler, A. A. Mitioglu, M. V. Ballottin, P. Nagler, A. V. Stier, T. Taniguchi, K. Watanabe, S. A. Crooker, P. C. M. Christianen, T. Korn, and A. Chernikov, Phys. Rev. B **98**, 075438 (2018).
[24]D. V. Rybkovskiy, I. C. Gerber, and M. V. Durnev, Phys. Rev. B **95**, 155406 (2017).
[25]T. Woźniak, P. E. Faria Junior, G. Seifert, A. Chaves, and J. Kunstmann, Phys. Rev. B **101**, 235408 (2020).
[26]J. Lindlau, M. Selig, A. Neumann, L. Colombier, J. Förste, V. Funk, M. Förg, J. Kim, G. Berghäuser, T. Taniguchi, K. Watanabe, F. Wang, E. Malic, and A. Högele, Nat. Commun. **9**, 2586 (2018).
[27]K. L. Seyler, P. Rivera, H. Yu, N. P. Wilson, E. L. Ray, D. G. Mandrus, J. Yan, W. Yao, and X. Xu, Nature **567**, 66 (2019).
[28]C. E. Stevens, J. Paul, T. Cox, P. K. Sahoo, H. R. Gutiérrez, V. Turkowski, D. Semenov, S. A. McGill, M. D. Kapetanakis, I. E. Perakis, D. J. Hilton, and D. Karaiskaj, Nat. Commun. **9**, 3720 (2018).
[29]H. Haug and S. W. Koch, *Quantum Theory of the Optical and Electronic Properties of Semiconductors* (World Scientific, 2009).
[30]T. Meier, P. Thomas, and S. W. Koch, *Coherent Semiconductor Optics* (Springer, 2007).
[31]J. Shah, *Ultrafast Spectroscopy of Semiconductors and Semiconductor Nanostructures* (Springer-Verlag, 1999).
[32]K. Leo, M. Wegener, J. Shah, D. S. Chemla, E. O. Göbel, T. C. Damen, S. Schmitt-Rink, and W. Schäfer, Phys. Rev. Lett. **65**, 1340 (1990).
[33]P. Kner, S. Bar-Ad, M. V. Marquezini, D. S. Chemla, and W. Schäfer, Phys. Rev. Lett. **78**, 1319 (1997).
[34]P. Kner, S. Bar-Ad, M. V. Marquezini, D. S. Chemla, R. Lövenich, and W. Schäfer, Phys. Rev. B **60**, 4731 (1999).
[35]D. S. Chemla and J. Shah, Nature **411**, 549 (2001).
[36]N. A. Fromer, C. Schüller, D. S. Chemla, T. V. Shahbazyan, I. E. Perakis, K. Maranowski, and A. C. Gossard, Phys. Rev. Lett. **83**, 4646 (1999).
[37]N. A. Fromer, C. Schüller, C. W. Lai, D. S. Chemla, I. E. Perakis, D. Driscoll, and A. C. Gossard, Phys. Rev. B **66**, 205314 (2002).
[38]Y. E. Lozovik, I. V. Ovchinnikov, S. Y. Volkov, L. V. Butov, and D. S. Chemla, Phys. Rev. B **65**, 235304 (2002).
[39]N. A. Fromer, C. E. Lai, D. S. Chemla, I. E. Perakis, D. Driscoll, and A. C. Gossard, Phys. Rev. Lett. **89**, 067401 (2002).
[40]K. M. Dani, J. Tignon, M. Breit, D. S. Chemla, E. G. Kavousanaki, and I. E. Perakis, Phys. Rev. Lett. **97**, 057401 (2006).
[41]A. T. Karathanos, I. E. Perakis, N. A. Fromer, and D. S. Chemla, Phys. Rev. B **67**, 035316 (2003).
[42]K. M. Dani, I. A. Cotoros, J. Wang, J. Tignon, D. S. Chemla, E. G. Kavousanaki, and I. E. Perakis, Phys. Rev. B **78**, 041301 (2008).
[43]R. A. Kaindl, D. Hägele, M. A. Carnahan, and D. S. Chemla, Phys. Rev. B **79**, 045320 (2009).
[44]J. Paul, C. E. Stevens, R. P. Smith, P. Dey, V. Mapara, D. Semenov, S. A. McGill, R. A. Kaindl, D. J. Hilton, and D. Karaiskaj, Rev. Sci. Instrum. **90**, 063901 (2019).
[45]J. Paul, C. E. Stevens, H. Zhang, P. Dey, D. McGinty, S. A. McGill, R. P. Smith, J. L. Reno, V. Turkowski, I. E. Perakis, D. J. Hilton, and D. Karaiskaj, Phys. Rev. B **95**, 245314 (2017).
[46]D. Karaiskaj, A. D. Bristow, L. Yang, X. Dai, R. P. Mirin, S. Mukamel, and S. T. Cundiff, Phys. Rev. Lett. **104**, 117401 (2010).
[47]K. W. Stone, K. Gundogdu, D. B. Turner, X. Li, S. T. Cundiff, and K. A. Nelson, Science **324**, 1169 (2009).
[48]D. B. Turner and K. A. Nelson, Nature **466**, 1089 (2010).
[49]P. Dey, J. Paul, N. Glikin, Z. D. Kovalyuk, Z. R. Kudrynskyi, A. H. Romero, and D. Karaiskaj, Phys. Rev. B **89**, 125128 (2014).
[50]P. Dey, J. Paul, G. Moody, C. E. Stevens, N. Glikin, Z. D. Kovalyuk, Z. R. Kudrynskyi, A. H. Romero, A. Cantarero, D. J. Hilton, and D. Karaiskaj, J. Chem. Phys. **142**, 212422 (2015).
[51]P. Dey, J. Paul, Z. Wang, C. E. Stevens, C. Liu, A. H. Romero, J. Shan, D. J. Hilton, and D. Karaiskaj, Phys. Rev. Lett. **116**, 127402 (2016).
[52]J. Paul, C. E. Stevens, C. Liu, P. Dey, C. McIntyre, V. Turkowski, J. L. Reno, D. J. Hilton, and D. Karaiskaj, Phys. Rev. Lett. **116**, 157401 (2016).
[53]J. Bylsma, P. Dey, J. Paul, S. Hoogland, E. H. Sargent, J. M. Luther, M. C. Beard, and D. Karaiskaj, Phys. Rev. B **86**, 125322 (2012).
[54]G. Moody and S. T. Cundiff, Adv. Phys. **2**, 641 (2017).
[55]P. Dey, J. Paul, J. Bylsma, S. Deminico, and D. Karaiskaj, Rev. Sci. Instrum. **84**, 023107 (2013).
[56]A. D. Bristow, D. Karaiskaj, X. Dai, T. Zhang, C. Carlsson, K. R. Hagen, R. Jimenez, and S. T. Cundiff, Rev. Sci. Instrum. **80**, 073108 (2009).
[57]S. T. Cundiff, Opt. Express **16**, 4639 (2008).
[58]S. Mukamel, *Principles of Nonlinear Optical Spectroscopy* (Oxford University Press, 1995).
[59]X. Li, T. Zhang, C. N. Borca, and S. T. Cundiff, Phys. Rev. Lett. **96**, 057406 (2006).
[60]D. M. Jonas, Annu. Rev. Phys. Chem. **54**, 425 (2003).
[61]J. Kim, S. Mukamel, and G. D. Scholes, Acc. Chem. Res. **42**, 1375 (2009).
[62]S. Mukamel, D. Abramavicius, L. Yang, W. Zhuang, I. V. Schweigert, and D. V. Voronine, Acc. Chem. Res. **42**, 553 (2009).
[63]S. Mukamel, Y. Tanimura, and P. Hamm, Acc. Chem. Res. **42**, 1207 (2009).
[64]M. Cho, *Two-Dimensional Optical Spectroscopy* (CRC Press, 2010), p. 378.
[65]P. Hamm and M. Zanni, *Concepts and Methods of 2D Infrared Spectroscopy* (Cambridge University Press, 2011), p. 286.
[66]Y. Onodera and Y. Toyozawa, J. Phys. Soc. Jpn. **22**, 833 (1967).
[67]F. Willmann, S. Suga, W. Dreybrodt, and K. Cho, Solid State Commun. **14**, 783 (1974).
[68]D. D. Sell, S. E. Stokowski, R. Dingle, and J. V. DiLorenzo, Phys. Rev. B **7**, 4568 (1973).
[69]W. Ekardt, K. Lösch, and D. Bimberg, Phys. Rev. B **20**, 3303 (1979).
[70]H. Fu, L.-W. Wang, and A. Zunger, Phys. Rev. B **59**, 5568 (1999).
[71]R. Dingle, Phys. Rev. B **8**, 4627 (1973).
[72]M. Altarelli and N. O. Lipari, Phys. Rev. B **9**, 1733 (1974).
[73]K. Cho, S. Suga, W. Dreybrodt, and F. Willmann, Phys. Rev. B **11**, 1512 (1975).
[74]S. B. Nam, D. C. Reynolds, C. W. Litton, R. J. Almassy, T. C. Collins, and C. M. Wolfe, Phys. Rev. B **13**, 761 (1976).
[75]K. K. Bajaj and C. H. Aldrich, Solid State Commun. **35**, 163 (1980).
[76]J. C. Maan, G. Belle, A. Fasolino, M. Altarelli, and K. Ploog, Phys. Rev. B **30**, 2253 (1984).

[77]D. C. Rogers, J. Singleton, R. J. Nicholas, C. T. Foxon, and K. Woodbridge, Phys. Rev. B **34**, 4002 (1986).
[78]F. H. Pollak and M. Cardona, Phys. Rev. **172**, 816 (1968).
[79]M. Chandrasekhar and F. H. Pollak, Phys. Rev. B **15**, 2127 (1977).
[80]T. Cheiwchanchamnangij and W. R. L. Lambrecht, Phys. Rev. B **84**, 035203 (2011).
[81]D. D. Sell, Phys. Rev. B **6**, 3750 (1972).
[82]B. L. Wilmer, D. Webber, J. M. Ashley, K. C. Hall, and A. D. Bristow, Phys. Rev. B **94**, 075207 (2016).
[83]D. Webber, B. L. Wilmer, X. Liu, M. Dobrowolska, J. K. Furdyna, A. D. Bristow, and K. C. Hall, Phys. Rev. B **94**, 155450 (2016).
[84]A. D. Bristow, D. Karaiskaj, X. Dai, R. P. Mirin, and S. T. Cundiff, Phys. Rev. B **79**, 161305 (2009).
[85]L. Yang, I. V. Schweigert, S. T. Cundiff, and S. Mukamel, Phys. Rev. B **75**, 125302 (2007).
[86]L. Yang and S. Mukamel, Phys. Rev. Lett. **100**, 057402 (2008).
[87]L. Yang and S. Mukamel, Phys. Rev. B **77**, 075335 (2008).
[88]M. Altarelli and N. O. Lipari, Phys. Rev. B **7**, 3798 (1973).
[89]C. M. N. Mateo, A. T. Garcia, F. R. M. Ramos, K. I. Manibog, and A. A. Salvador, J. Appl. Phys. **101**, 073519 (2007).
[90]Y. Sun, S. E. Thompson, and T. Nishida, J. Appl. Phys. **101**, 104503 (2007).
[91]C. M. N. Mateo, J. J. Ibañez, J. G. Fernando, J. C. Garcia, K. Omambac, R. B. Jaculbia, M. Defensor, and A. A. Salvador, J. Appl. Phys. **104**, 103537 (2008).
[92]M. E. Siemens, G. Moody, H. Li, A. D. Bristow, and S. T. Cundiff, Opt. Express **18**, 17699 (2010).
[93]B. Lomsadze and S. T. Cundiff, Phys. Rev. A **102**, 043514 (2020).